Provided for non-commercial research and education use.
Not for reproduction, distribution or commercial use.

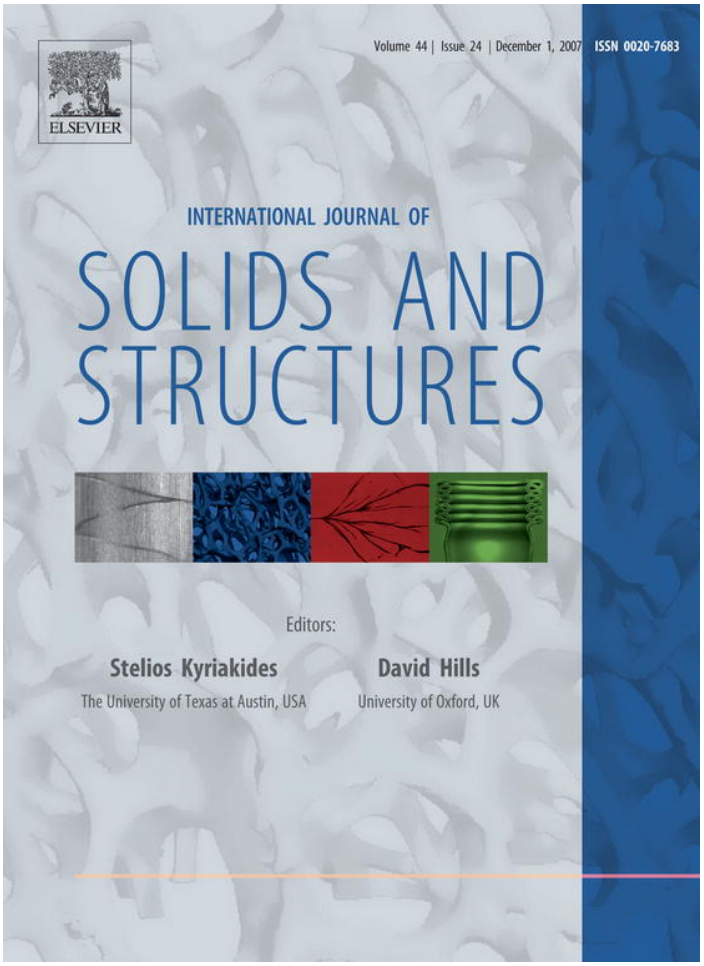

This article was published in an Elsevier journal. The attached copy is furnished to the author for non-commercial research and education use, including for instruction at the author's institution, sharing with colleagues and providing to institution administration.

Other uses, including reproduction and distribution, or selling or licensing copies, or posting to personal, institutional or third party websites are prohibited.

In most cases authors are permitted to post their version of the article (e.g. in Word or Tex form) to their personal website or institutional repository. Authors requiring further information regarding Elsevier's archiving and manuscript policies are encouraged to visit:

http://www.elsevier.com/copyright

Author's personal copy

Available online at www.sciencedirect.com
ScienceDirect
International Journal of Solids and Structures 44 (2007) 7955–7974
INTERNATIONAL JOURNAL OF SOLIDS AND STRUCTURES
www.elsevier.com/locate/ijsolstr

Dynamic fracture analysis of a penny-shaped crack in a magnetoelectroelastic layer

W.J. Feng [a,b,*], E. Pan [b], X. Wang [b]

[a] Department of Engineering Mechanics, Shijiazhuang Railway Institute, Shijiazhuang 050043, P.R. China
[b] Department of Civil Engineering, The University of Akron, Akron, OH 44325-3905, USA

Received 21 February 2007; received in revised form 25 April 2007
Available online 2 June 2007

Abstract

This paper analyzes the dynamic magnetoelectroelastic behavior induced by a penny-shaped crack in a magnetoelectroelastic layer subjected to prescribed stress or prescribed displacement at the layer surfaces. Two kinds of crack surface conditions, i.e., magnetoelectrically impermeable and permeable cracks, are adopted. The Laplace and Hankel transform techniques are employed to reduce the problem to Fredholm integral equations. Field intensity factors are obtained and discussed. Numerical results of the crack opening displacement (COD) intensity factors are presented and the effects of magnetoelectromechanical loadings, crack surface conditions and crack configuration on crack propagation and growth are examined. The results indicate that among others, the fracture behaviors of magnetoelectroelastic materials are affected by the sizes and directions of the prescribed magnetic and/or electric fields, and the effects are strongly dependent on the elastic boundary conditions.
© 2007 Elsevier Ltd. All rights reserved.

Keywords: Magnetoelectroelastic layer; Penny-shaped crack; Impact; COD intensity factor; Magnetoelectrically impermeable (permeable) crack; Hankel transform; Laplace transform

1. Introduction

Materials possessing magnetoelectroelastic coupling effects have found increasing applications in engineering structures, particularly in smart materials/intelligent structures. The effects of magnetoelectromechanical coupling have been observed in single-phase materials where simultaneous magnetic and electric ordering coexists, and in two-phase composites where the participating phases are piezoelectric and piezomagnetic (Avellaneda and Harshe, 1994; Benveniste, 1995; Harshe et al., 1993; Huang and Kuo, 1997; Kirchner and Alshits, 1996; Li and Dunn, 1998; Nan, 1994). In recent years, an area of increasing interest is the fracture mechanics of magnetoelectroelastic materials, which combine the ferromagnetic and ferroelectric phases, and most of the

* Corresponding author. Address: Department of Engineering Mechanics, Shijiazhuang Railway Institute, Shijiazhuang 050043, P.R. China. Tel.: +86 311 87936543; fax: +86 311 87935169.
E-mail address: wjfeng999@yahoo.com (W.J. Feng).

0020-7683/$ - see front matter © 2007 Elsevier Ltd. All rights reserved.
doi:10.1016/j.ijsolstr.2007.05.020

Author's personal copy

achievements are made on anti-plane problems (Zhou et al., 2004; Hu et al., 2006; Wang et al., 2006; Li and Kardomateas, 2006) and two dimensional in-plane problems (Song and Sih, 2003; Gao et al., 2003; Tian and Gabbert, 2004; Sih and Yu, 2005; Soh and Liu, 2005; Tian and Gabbert, 2005; Tian and Rajapakse, 2005; Chue and Liu, 2005; Wang and Mai, 2007) under static deformation assumption. However, to date, the analysis of dynamic fracture problems of magnetoelectroelastic materials is very limited (Du et al., 2004; Feng and Su, 2006; Su et al., 2007), not to mention that, all the progresses have been made only on anti-plane problems.

On the other hand, more recently, the penny-shaped crack in a magnetoelectroelastic material has been considered. For example, Zhao et al. (2006) analyzed a penny-shaped crack in a magnetoelectroelastic medium. Niraula and Wang (2006) derived an exact closed-form solution for a penny-shaped crack in a magneto-electrothermoelastic material in a temperature field. However, all of the studies considered only static problems and infinite magnetoelectroelastic body. To the best of our knowledge, the penny-shaped crack problems under dynamic loads in the coupled magnetoelectroelastic material have not been addressed yet, especially for a finite magnetoelectroelastic body.

In this paper, the transient response of a penny-shaped crack embedded in a magnetoelectroelastic layer of finite thickness is considered. Two impact cases are studied, one corresponding to prescribed stress at the layer surfaces and the other to prescribed displacement. The crack surface is assumed magnetoelectrically impermeable or permeable. By means of the Laplace and Hankel transform techniques, the problem is reduced to Fredholm integral equations with respect to unknown auxiliary functions in the Laplace domain. Field intensity factors are obtained and discussed in detail. Numerical calculations are carried out and the effects of both applied magnetic and electric fields on the COD intensity factors are presented graphically for various loading and crack surface cases.

2. Statement of the problem

Consider a class of axisymmetric problems of a transversely isotropic magnetroelectroelastic layer of thickness $2h$ with the poling direction along the z-axis and the isotropic plane as the xy-plane. The constitutive equations within the framework of the theory of linear magnetoelectroelastic medium take the form

$$\begin{Bmatrix}\sigma_{rr}\\ \sigma_{\theta\theta}\\ \sigma_{zz}\\ \sigma_{rz}\end{Bmatrix}=\begin{bmatrix}c_{11}&c_{12}&c_{13}&0\\ c_{12}&c_{11}&c_{13}&0\\ c_{13}&c_{13}&c_{33}&0\\ 0&0&0&c_{44}\end{bmatrix}\begin{Bmatrix}\frac{\partial u_r}{\partial r}\\ \frac{u_r}{r}\\ \frac{\partial u_z}{\partial z}\\ \frac{\partial u_r}{\partial z}+\frac{\partial u_z}{\partial r}\end{Bmatrix}+\begin{bmatrix}0&e_{31}\\ 0&e_{31}\\ 0&e_{33}\\ e_{15}&0\end{bmatrix}\begin{Bmatrix}\frac{\partial \phi}{\partial r}\\ \frac{\partial \phi}{\partial z}\end{Bmatrix}+\begin{bmatrix}0&f_{31}\\ 0&f_{31}\\ 0&f_{33}\\ f_{15}&0\end{bmatrix}\begin{Bmatrix}\frac{\partial \psi}{\partial r}\\ \frac{\partial \psi}{\partial z}\end{Bmatrix}, \tag{1a}$$

$$\begin{Bmatrix}D_r\\ D_z\end{Bmatrix}=\begin{bmatrix}0&0&0&e_{15}\\ e_{31}&e_{31}&e_{33}&0\end{bmatrix}\begin{Bmatrix}\frac{\partial u_r}{\partial r}\\ \frac{u_r}{r}\\ \frac{\partial u_z}{\partial z}\\ \frac{\partial u_r}{\partial z}+\frac{\partial u_z}{\partial r}\end{Bmatrix}-\begin{bmatrix}\varepsilon_{11}&0\\ 0&\varepsilon_{33}\end{bmatrix}\begin{Bmatrix}\frac{\partial \phi}{\partial r}\\ \frac{\partial \phi}{\partial z}\end{Bmatrix}-\begin{bmatrix}g_{11}&0\\ 0&g_{33}\end{bmatrix}\begin{Bmatrix}\frac{\partial \psi}{\partial r}\\ \frac{\partial \psi}{\partial z}\end{Bmatrix}, \tag{1b}$$

$$\begin{Bmatrix}B_r\\ B_z\end{Bmatrix}=\begin{bmatrix}0&0&0&f_{15}\\ f_{31}&f_{31}&f_{33}&0\end{bmatrix}\begin{Bmatrix}\frac{\partial u_r}{\partial r}\\ \frac{u_r}{r}\\ \frac{\partial u_z}{\partial z}\\ \frac{\partial u_r}{\partial z}+\frac{\partial u_z}{\partial r}\end{Bmatrix}-\begin{bmatrix}g_{11}&0\\ 0&g_{33}\end{bmatrix}\begin{Bmatrix}\frac{\partial \phi}{\partial r}\\ \frac{\partial \phi}{\partial z}\end{Bmatrix}-\begin{bmatrix}\mu_{11}&0\\ 0&\mu_{33}\end{bmatrix}\begin{Bmatrix}\frac{\partial \psi}{\partial r}\\ \frac{\partial \psi}{\partial z}\end{Bmatrix}, \tag{1c}$$

where the field quantities are functions of r and z, independent of angle θ; u_r and u_z are radial and axial components of elastic displacements; ϕ and ψ are electric potential and magnetic potential; σ_{ij}, D_i and B_i are stresses, electric displacements and magnetic inductions; c_{ij}, e_{ij}, f_{ij} and g_{ij} are elastic, piezoelectric, piezomagnetic and magnetoelectric constants; ε_{ij} and μ_{ij} are dielectric permittivities and magnetic permeabilities.

In the absence of body forces, electric and magnetic charge densities, stresses, electric displacements and magnetic inductions satisfy the following equations:

Author's personal copy

$$\frac{\partial \sigma_{rr}}{\partial r}+\frac{\partial \sigma_{rz}}{\partial z}+\frac{\sigma_{rr}-\sigma_{\theta\theta}}{r}=\rho\frac{\partial^2 u_r}{\partial t^2}, \tag{2a}$$

$$\frac{\partial \sigma_{rz}}{\partial r}+\frac{\partial \sigma_{zz}}{\partial z}+\frac{\sigma_{rz}}{r}=\rho\frac{\partial^2 u_z}{\partial t^2}, \tag{2b}$$

$$\frac{\partial D_r}{\partial r}+\frac{\partial D_z}{\partial z}+\frac{D_r}{r}=0, \tag{2c}$$

$$\frac{\partial B_r}{\partial r}+\frac{\partial B_z}{\partial z}+\frac{B_r}{r}=0, \tag{2d}$$

where ρ is the material density and t denotes time.

Substituting the constitutive Eq. (1) into the above equations yields the basic governing equations for the elastic displacements u_r and u_z, electric potential ϕ, and magnetic potential ψ as follows

$$c_{11}\left(\frac{\partial^2 u_r}{\partial r^2}+\frac{1}{r}\frac{\partial u_r}{\partial r}-\frac{u_r}{r^2}\right)+c_{44}\frac{\partial^2 u_r}{\partial z^2}+(c_{13}+c_{44})\frac{\partial^2 u_z}{\partial r\partial z}+(e_{31}+e_{15})\frac{\partial^2 \phi}{\partial r\partial z}+(f_{31}+f_{15})\frac{\partial^2 \psi}{\partial r\partial z}=\rho\frac{\partial^2 u_r}{\partial t^2}, \tag{3a}$$

$$\begin{aligned}&c_{44}\left(\frac{\partial^2 u_z}{\partial r^2}+\frac{1}{r}\frac{\partial u_z}{\partial r}\right)+c_{33}\frac{\partial^2 u_z}{\partial z^2}+(c_{13}+c_{44})\left(\frac{\partial^2 u_r}{\partial r\partial z}+\frac{1}{r}\frac{\partial u_r}{\partial z}\right)+e_{15}\left(\frac{\partial^2 \phi}{\partial r^2}+\frac{1}{r}\frac{\partial \phi}{\partial r}\right)+e_{33}\frac{\partial^2 \phi}{\partial z^2}\\&+f_{15}\left(\frac{\partial^2 \psi}{\partial r^2}+\frac{1}{r}\frac{\partial \psi}{\partial r}\right)+f_{33}\frac{\partial^2 \psi}{\partial z^2}=\rho\frac{\partial^2 u_z}{\partial t^2},\end{aligned} \tag{3b}$$

$$\begin{aligned}&(e_{31}+e_{15})\left(\frac{\partial^2 u_r}{\partial r\partial z}+\frac{1}{r}\frac{\partial u_r}{\partial z}\right)+e_{15}\left(\frac{\partial^2 u_z}{\partial r^2}+\frac{1}{r}\frac{\partial u_z}{\partial r}\right)+e_{33}\frac{\partial^2 u_z}{\partial z^2}-\varepsilon_{11}\left(\frac{\partial^2 \phi}{\partial r^2}+\frac{1}{r}\frac{\partial \phi}{\partial r}\right)-\varepsilon_{33}\frac{\partial^2 \phi}{\partial z^2}\\&-g_{11}\left(\frac{\partial^2 \psi}{\partial r^2}+\frac{1}{r}\frac{\partial \psi}{\partial r}\right)-g_{33}\frac{\partial^2 \psi}{\partial z^2}=0,\end{aligned} \tag{3c}$$

$$\begin{aligned}&(f_{31}+f_{15})\left(\frac{\partial^2 u_r}{\partial r\partial z}+\frac{1}{r}\frac{\partial u_r}{\partial z}\right)+f_{15}\left(\frac{\partial^2 u_z}{\partial r^2}+\frac{1}{r}\frac{\partial u_z}{\partial r}\right)+f_{33}\frac{\partial^2 u_z}{\partial z^2}-g_{11}\left(\frac{\partial^2 \phi}{\partial r^2}+\frac{1}{r}\frac{\partial \phi}{\partial r}\right)-g_{33}\frac{\partial^2 \phi}{\partial z^2}\\&-\mu_{11}\left(\frac{\partial^2 \psi}{\partial r^2}+\frac{1}{r}\frac{\partial \psi}{\partial r}\right)-\mu_{33}\frac{\partial^2 \psi}{\partial z^2}=0.\end{aligned} \tag{3d}$$

In what follows, special attention is focused on determining magnetoelectroelastic behaviors of a cracked transversely isotropic magnetoelectroelastic layer under magnetoelectromechanical impact loadings. It is assumed that a flat penny-shaped crack of radius a perpendicular to the poling axis is situated at the mid-plane of the layer and occupies the region $r \leqslant a$, $z = 0$, as shown in Fig. 1. For convenience, two possible cases of magnetoelectromechanical loadings applied to the layer surfaces are considered: one corresponding to the prescribed impacts of elastic stress, electric field and magnetic field, and the other to the prescribed impacts of elastic displacement, electric potential and magnetic potential. In other words,

$$\text{Case A: } \sigma_{zz}(r,\pm h,t)=\sigma_0 H(t), u_r(r,\pm h,t)=0, \quad r<\infty, \tag{4a}$$

$$E_z(r,\pm h,t)=E_0 H(t), H_z(r,\pm h,t)=H_0 H(t), \quad r<\infty, \tag{4b}$$

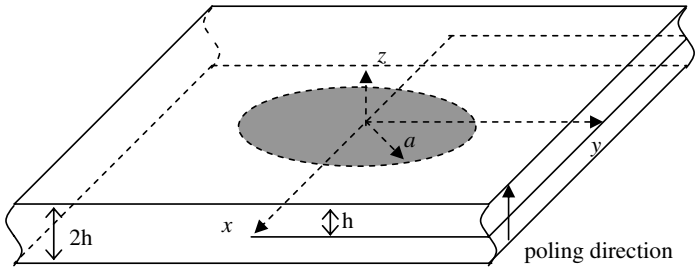

Fig. 1. Geometry of a magnetoelectroelastic layer with a horizontal, central, and penny-shaped crack.

Author's personal copy

$$\text{Case B: } u_z(r,\pm h,t)=\pm u_h H(t),\ \sigma_{rz}(r,\pm h,t)=0,\quad r<\infty, \tag{5a}$$

$$\phi(r,\pm h,t)=\mp\phi_h H(t),\ \psi(r,\pm h,t)=\mp\psi_h H(t),\quad r<\infty, \tag{5b}$$

where σ_0, u_h, E_0, ϕ_h, B_0 and ψ_h are given constants, $H(t)$ is the Heaviside function.

In this study, two kinds of magnetoelectric crack surface conditions are adopted, i.e., magnetoelectrically impermeable and permeable. For simplicity, they are identically expressed as

$$\sigma_{zz}(r,0,t)=0,\ \sigma_{zr}(r,0,t)=0,\ D_z(r,0,t)=d_0(t),\ B_z(r,0,t)=b_0(t),\ r<a, \tag{6}$$

where for the magnetoelectrically impermeable crack case, both d_0 and b_0 vanish, whilst for the corresponding permeable case, both d_0 and b_0 are unknown to be determined.

3. Magnetoelectrically impermeable cracks

3.1. Derivation of Fredholm integral equations

Because of the symmetry of the problem, it is sufficient to consider the upper-half space of the penny-shaped crack. By introducing the Laplace transform, the boundary conditions in Laplace domain can be expressed as

$$\text{Case A: } \sigma^*_{zz}(r,h,p)=\frac{\sigma_0}{p},\quad u^*_r(r,h,p)=0,\quad E^*_z(r,h,p)=\frac{E_0}{p},\quad H^*_z(r,h,p)=\frac{H_0}{p},\quad r<\infty, \tag{7}$$

$$\text{Case B: } u^*_z(r,h,p)=\frac{u_h}{p},\quad \sigma^*_{rz}(r,h,p)=0,\quad \phi^*(r,h,p)=-\frac{\phi_h}{p},\quad \psi^*(r,h,p)=-\frac{\psi_h}{p},\quad r<\infty \tag{8}$$

on the upper surface of the layer, and

$$\sigma^*_{zz}(r,0,p)=0,\quad \sigma^*_{zr}(r,0,p)=0,\quad D^*_z(r,0,p)=d^*_0(p),\quad B^*_z(r,0,p)=b^*_0(p),\quad r<a, \tag{9}$$

$$u^*_z(r,0,p)=0,\quad \sigma^*_{zr}(r,0,p)=0,\quad \phi^*(r,0,p)=0,\quad \psi^*(r,0,p)=0,\quad r\geqslant a \tag{10}$$

on the $z=0$ plane (i.e., the crack plane). We remark that for the magneoelectrically impermeable crack, both $d^*_0(p)$ and $b^*_0(p)$ vanish.

By further introducing the Hankel transform and considering the boundary conditions in Eq. (7) and/or (8), the general expressions for the elastic displacements, electric potential and magnetic potential in terms of unknown functions A_j and B_j ($j=1, 2, 3, 4$) in the Laplace domain can be found as follows:

$$u^*_r(r,z,p)=\sum_{j=1}^{4}\int_0^\infty [A_j(\xi,p)\sinh(\gamma_j\xi z)+B_j(\xi,p)\cosh(\gamma_j\xi z)]J_1(\xi r)\mathrm{d}\xi, \tag{11a}$$

$$u^*_z(r,z,p)=-\sum_{j=1}^{4}\int_0^\infty \eta_{1j}\gamma_j[A_j(\xi,p)\cosh(\gamma_j\xi z)+B_j(\xi,p)\sinh(\gamma_j\xi z)]J_0(\xi r)\mathrm{d}\xi+a_0 z/p, \tag{11b}$$

$$\phi^*(r,z,p)=-\sum_{j=1}^{4}\int_0^\infty \eta_{2j}\gamma_j[A_j(\xi,p)\cosh(\gamma_j\xi z)+B_j(\xi,p)\sinh(\gamma_j\xi z)]J_0(\xi r)\mathrm{d}\xi-b_0 z/p, \tag{11c}$$

$$\psi^*(r,z,p)=-\sum_{j=1}^{4}\int_0^\infty \eta_{3j}\gamma_j[A_j(\xi,p)\cosh(\gamma_j\xi z)+B_j(\xi,p)\sinh(\gamma_j\xi z)]J_0(\xi r)\mathrm{d}\xi-c_0 z/p, \tag{11d}$$

where γ_j ($j=1, 2, 3, 4$) and η_{ij}($i=1, 2, 3$, $j=1, 2, 3, 4$) are material constants dependent on both the Laplace and Hankel transform parameters. Other constants a_0, b_0 and c_0 can easily be obtained from Eqs. (7) and (8) as

$$a_0=(\sigma_0+e_{33}E_0+f_{33}H_0)/c_{33},\quad b_0=E_0,\quad c_0=H_0 \tag{12}$$

for Case A, and

$$a_0=u_h/h,\quad b_0=\phi_h/h,\quad c_0=\psi_h/h \tag{13}$$

Author's personal copy

for Case B.

Substituting Eq. (11) into Eq. (3), it is found that γ_j satisfies the following characteristic equation:

$$\det(\mathbf{M}) = 0, \tag{14}$$

and that $\eta_{ij}(p/\xi)$ are known constants satisfying the following relations:

$$\mathbf{M}\{\ 1 \quad -\eta_{1j}\gamma_j \quad -\eta_{2j}\gamma_j \quad -\eta_{3j}\gamma_j\ \}^{\mathrm{T}} = 0, \tag{15}$$

where

$$\mathbf{M}(p/\xi) = \begin{bmatrix} c_{11} - c_{44}\gamma_j^2 + \rho p^2/\xi^2 & (c_{13} + c_{44})\gamma_j & (e_{31} + e_{15})\gamma_j & (f_{31} + f_{15})\gamma_j \\ (c_{13} + c_{44})\gamma_j & c_{33}\gamma_j^2 - c_{44} - \rho p^2/\xi^2 & e_{33}\gamma_j^2 - e_{15} & f_{33}\gamma_j^2 - f_{15} \\ (e_{31} + e_{15})\gamma_j & e_{33}\gamma_j^2 - e_{15} & \varepsilon_{11} - \varepsilon_{33}\gamma_j^2 & g_{11} - g_{33}\gamma_j^2 \\ (f_{31} + f_{15})\gamma_j & f_{33}\gamma_j^2 - f_{15} & g_{11} - g_{33}\gamma_j^2 & \mu_{11} - \mu_{33}\gamma_j^2 \end{bmatrix}. \tag{16}$$

It should be pointed out that Eq. (14) has eight roots for given material constants together with the Laplace and Hankel transform parameters, and that if $\gamma(p/\xi)$ is a root, $-\gamma(p/\xi)$ is also a root of the equation. In other words, only four of them are independent. Thus, in this paper, $\gamma_j(p/\xi)$ are chosen such that $\mathrm{Re}(\gamma_j)$ are larger than zero.

From the constitutive equations, the expressions for the stresses, electric displacement and magnetic induction in terms of A_j and B_j in the Laplace domain can also be obtained. They are

$$\sigma_{zz}^*(r,z,p) = -\sum_{j=1}^{4}\int_0^\infty \beta_{1j}\xi[A_j(\xi,p)\sinh(\gamma_j\xi z) + B_j(\xi,p)\cosh(\gamma_j\xi z)]J_0(\xi r)\mathrm{d}\xi + \bar{\sigma}_0/p, \tag{17a}$$

$$\sigma_{rz}^*(r,z,p) = \sum_{j=1}^{4}\int_0^\infty \beta_{2j}\xi[A_j(\xi,p)\cosh(\gamma_j\xi z) + B_j(\xi,p)\sinh(\gamma_j\xi z)]J_1(\xi r)\mathrm{d}\xi, \tag{17b}$$

$$D_z^*(r,z,p) = -\sum_{j=1}^{4}\int_0^\infty \beta_{3j}\xi[A_j(\xi,p)\sinh(\gamma_j\xi z) + B_j(\xi,p)\cosh(\gamma_j\xi z)]J_0(\xi r)\mathrm{d}\xi + \bar{D}_0/p, \tag{17c}$$

$$B_z^*(r,z,p) = -\sum_{j=1}^{4}\int_0^\infty \beta_{4j}\xi[A_j(\xi,p)\sinh(\gamma_j\xi z) + B_j(\xi,p)\cosh(\gamma_j\xi z)]J_0(\xi r)\mathrm{d}\xi + \bar{B}_0/p, \tag{17d}$$

where

$$\beta_{1j}(p/\xi) = [c_{33}\eta_{1j}(p/\xi) + e_{33}\eta_{2j}(p/\xi) + f_{33}\eta_{3j}(p/\xi)]\gamma_j^2(p/\xi) - c_{13}, \tag{18a}$$

$$\beta_{2j}(p/\xi) = [c_{44}(1 + \eta_{1j}(p/\xi)) + e_{15}\eta_{2j}(p/\xi) + f_{15}\eta_{3j}(p/\xi)]\gamma_j(p/\xi), \tag{18b}$$

$$\beta_{3j}(p/\xi) = (e_{33}\eta_{1j}(p/\xi) - \varepsilon_{33}\eta_{2j}(p/\xi) - g_{33}\eta_{3j}(p/\xi))\gamma_j^2(p/\xi) - e_{31}, \tag{18c}$$

$$\beta_{4j}(p/\xi) = (f_{33}\eta_{1j}(p/\xi) - g_{33}\eta_{2j}(p/\xi) - \mu_{33}\eta_{3j}(p/\xi))\gamma_j^2(p/\xi) - f_{31}. \tag{18d}$$

Also in Eq. (17),

$$\bar{\sigma}_0 = \sigma_0, \tag{19a}$$

$$\bar{D}_0 = \varepsilon_{33}E_0 + g_{33}H_0 + e_{33}(\sigma_0 + e_{33}E_0 + f_{33}H_0)/c_{33}, \tag{19b}$$

$$\bar{B}_0 = g_{33}E_0 + \mu_{33}H_0 + f_{33}(\sigma_0 + e_{33}E_0 + f_{33}H_0)/c_{33} \tag{19c}$$

for Case A, and

$$\bar{\sigma}_0 = c_{33}u_h/h - e_{33}\phi_h/h - f_{33}\psi_h/h, \tag{20a}$$

$$\bar{D}_0 = e_{33}u_h/h + \varepsilon_{33}\phi_h/h + g_{33}\psi_h/h, \tag{20b}$$

$$\bar{B}_0 = f_{33}u_h/h + g_{33}\phi_h/h + \mu_{33}\psi_h/h \tag{20c}$$

Author's personal copy

for Case B.

In fact, from the basic fracture mechanics, the problem considered here is equivalent to the one where $-\bar{\sigma}_0 H(t), -\bar{D}_0 H(t)$ and $-\bar{B}_0 H(t)$ are directly applied on the crack surfaces, and all the quantities on the left-hand sides of Eq. (4) for Case A and Eq. (5) for Case B are equal to zero. Thus, for convenience, in this study, $-\bar{\sigma}_0, -\bar{D}_0$ and $-\bar{B}_0$ are called, respectively, as mechanical, electrical and magnetic loadings applied on the crack surfaces.

3.1.1. Case A

We first consider Case A. For convenience, we denote the components of stress, electric displacement and magnetic induction on the crack plane $(z = 0)$ as $\sigma^*_{zz}(r,p) = \sigma^*_{zz}(r,0,p)$, $D^*_z(r,p) = D^*_z(r,0,p)$, $B^*_z(r,p) = B^*_z(r,0,p)$, respectively. Similarly, the components of the elastic displacement, electric potential and magnetic potential on the crack plane are denoted as $u^*_z(r,p)$, $\phi^*(r,p)$ and $\psi^*(r,p)$, respectively.

Substituting Eqs. (17a), (11a), (11c) and (11d) into Eq. (7) leads to

$$-\sum_{j=1}^{4}\int_0^\infty \beta_{1j}\xi[A_j(\xi,p)\sinh(\gamma_j\xi h) + B_j(\xi,p)\cosh(\gamma_j\xi h)]J_0(\xi r)\mathrm{d}\xi = 0, \tag{21a}$$

$$\sum_{j=1}^{4}\int_0^\infty [A_j(\xi,p)\sinh(\gamma_j\xi h) + B_j(\xi,p)\cosh(\gamma_j\xi h)]J_1(\xi r)\mathrm{d}\xi = 0, \tag{21b}$$

$$-\sum_{j=1}^{4}\int_0^\infty \eta_{2j}\gamma_j^2\xi[A_j(\xi,p)\sinh(\gamma_j\xi h) + B_j(\xi,p)\cosh(\gamma_j\xi h)]J_0(\xi r)\mathrm{d}\xi = 0, \tag{21c}$$

$$-\sum_{j=1}^{4}\int_0^\infty \eta_{3j}\gamma_j^2\xi[A_j(\xi,p)\sinh(\gamma_j\xi h) + B_j(\xi,p)\cosh(\gamma_j\xi h)]J_0(\xi r)\mathrm{d}\xi = 0. \tag{21d}$$

It is easily verified that the system has a unique solution

$$B_j(\xi,p) = -A_j(\xi,p)\tanh(\gamma_j\xi h), \quad j = 1,2,3,4. \tag{22}$$

On the other hand, from Eqs. (11b), (11c) and (11d), the displacement, electric potential and magnetic potential on the crack plane can be written as

$$u^*_z(r,p) = -\sum_{j=1}^{4}\int_0^\infty \eta_{1j}\gamma_j A_j(\xi,p)J_0(\xi r)\mathrm{d}\xi, \tag{23a}$$

$$\phi^*(r,p) = -\sum_{j=1}^{4}\int_0^\infty \eta_{2j}\gamma_j A_j(\xi,p)J_0(\xi r)\mathrm{d}\xi, \tag{23b}$$

$$\psi^*(r,p) = -\sum_{j=1}^{4}\int_0^\infty \eta_{3j}\gamma_j A_j(\xi,p)J_0(\xi r)\mathrm{d}\xi. \tag{23c}$$

To transform the mixed boundary value problem into integral equations, three new unknown functions $U(r,p)$, $\Phi(r,p)$ and $\Psi(r,p)$ are introduced, which satisfy the following equations:

$$\sum_{j=1}^{4}\eta_{1j}\gamma_j A_j(\xi,p) = -\int_0^a U(s,p)\sin(\xi s)\mathrm{d}s, \tag{24a}$$

$$\sum_{j=1}^{4}\eta_{2j}\gamma_j A_j(\xi,p) = -\int_0^a \Phi(s,p)\sin(\xi s)\mathrm{d}s, \tag{24b}$$

$$\sum_{j=1}^{4}\eta_{3j}\gamma_j A_j(\xi,p) = -\int_0^a \Psi(s,p)\sin(\xi s)\mathrm{d}s. \tag{24c}$$

Author's personal copy

Substituting Eq. (24) into Eq. (23), recalling the following known result (Abramowitz and Stegun, 1965)

$$\int_0^\infty J_0(\xi r)\sin(\xi s)\mathrm{d}\xi = \frac{H(s-r)}{\sqrt{s^2-r^2}}, \tag{25}$$

we find that the boundary conditions in Eqs. (10_1), (10_3) and (10_4) are automatically satisfied. Moreover, the displacement, electric potential and magnetic potential on the crack plane can be expressed in terms of the introduced unknown functions as

$$u_z^*(r,p) = \int_r^a \frac{U(s,p)}{\sqrt{s^2-r^2}}\mathrm{d}s, \quad \phi^*(r,p) = \int_r^a \frac{\Phi(s,p)}{\sqrt{s^2-r^2}}\mathrm{d}s, \quad \psi^*(r,p) = \int_r^a \frac{\Psi(s,p)}{\sqrt{s^2-r^2}}\mathrm{d}s, \quad r<a. \tag{26}$$

Next, Eq. (24) in connection with the application of Eqs. (9_2), (10_2) and (17b) form a system of linear algebraic equations for $A_j (j = 1, 2, 3, 4)$, from which we obtain

$$A_j(\xi,p) = -\alpha_{1j}(p/\xi)\int_0^a U(s,p)\sin(\xi s)\mathrm{d}s - \alpha_{2j}(p/\xi)\int_0^a \Phi(s,p)\sin(\xi s)\mathrm{d}s - \alpha_{3j}(p/\xi)\int_0^a \Psi(s)\sin(\xi s)\mathrm{d}s, \tag{27}$$

where

$$\alpha_{ij} = \bar{Q}_{ij}/\det(\mathbf{Q}), \quad i = 1, 2, 3, \quad j = 1, 2, 3, 4, \tag{28}$$

and $\mathbf{Q}$ is a 4×4 matrix with its elements being

$$Q_{ij}(p/\xi) = \eta_{ij}(p/\xi)\gamma_j(p/\xi), \quad i = 1, 2, 3, \quad j = 1, 2, 3, 4, \tag{29a}$$

$$\Omega_{4j}(p/\xi) = \beta_{2j}(p/\xi), \quad j = 1, 2, 3, 4, \tag{29b}$$

and $\bar{Q}_{ij}(p/\xi)$ are the corresponding algebraic cofactors of Q_{ij}. Inserting Eq. (27) into Eq. (22) and then into Eqs. (17a), (17c) and (17d) yields

$$\sigma_{zz}^*(r,p) = -\int_0^a\int_0^\infty [\widehat{m}_{11}U(s,p) + \widehat{m}_{12}\Phi(s,p) + \widehat{m}_{13}\Psi(s,p)]\xi\sin(\xi s)J_0(\xi r)\mathrm{d}\xi\mathrm{d}s + \bar{\sigma}_0/p, \tag{30a}$$

$$D_z^*(r,p) = -\int_0^a\int_0^\infty [\widehat{m}_{21}U(s,p) + \widehat{m}_{22}\Phi(s,p) + \widehat{m}_{23}\Psi(s,p)]\xi\sin(\xi s)J_0(\xi r)\mathrm{d}\xi\mathrm{d}s + \bar{D}_0/p, \tag{30b}$$

$$B_z^*(r,p) = -\int_0^a\int_0^\infty [\widehat{m}_{31}U(s,p) + \widehat{m}_{32}\Phi(s,p) + \widehat{m}_{33}\Psi(s,p)]\xi\sin(\xi s)J_0(\xi r)\mathrm{d}\xi\mathrm{d}s + \bar{B}_0/p, \tag{30c}$$

where

$$\widehat{m}_{1l}(\xi,p) = \sum_{j=1}^4 \beta_{1j}(p/\xi)\alpha_{lj}(p/\xi)\tanh(\gamma_j\xi h), \quad l = 1, 2, 3, \tag{31a}$$

$$\widehat{m}_{kl}(\xi,p) = \sum_{j=1}^4 \beta_{(k+1)j}(p/\xi)\alpha_{lj}(p/\xi)\tanh(\gamma_j\xi h), \quad k = 2, 3, \quad l = 1, 2, 3. \tag{31b}$$

Making use of the boundary conditions in Eqs. (9_1), (9_3), (9_4), we further obtain the following equations:

$$\int_0^a\int_0^\infty [\widehat{m}_{11}U(s,p) + \widehat{m}_{12}\Phi(s,p) + \widehat{m}_{13}\Psi(s,p)]\xi\sin(\xi s)J_0(\xi r)\mathrm{d}\xi\mathrm{d}s = \frac{\bar{\sigma}_0}{p}, \tag{32a}$$

$$\int_0^a\int_0^\infty [\widehat{m}_{21}U(s,p) + \widehat{m}_{22}\Phi(s,p) + \widehat{m}_{23}\Psi(s,p)]\xi\sin(\xi s)J_0(\xi r)\mathrm{d}\xi\mathrm{d}s = \frac{\bar{D}_0}{p}, \tag{32b}$$

$$\int_0^a\int_0^\infty [\widehat{m}_{31}U(s,p) + \widehat{m}_{32}\Phi(s,p) + \widehat{m}_{33}\Psi(s,p)]\xi\sin(\xi s)J_0(\xi r)\mathrm{d}\xi\mathrm{d}s = \frac{\bar{B}_0}{p}. \tag{32c}$$

Multiplying $r/(x^2-r^2)^{1/2}$ to two sides of Eqs. (32a), (32b) and (32c), integrating with respect to r from 0 to $x (x < a)$, respectively, and using the following identity (Abramowitz and Stegun, 1965)

Author's personal copy

$$\int_0^x \frac{rJ_0(\xi r)}{\sqrt{x^2-r^2}}\mathrm{d}r = \frac{\sin(\xi x)}{\xi}, \tag{33}$$

we finally obtain

$$\int_0^a \int_0^\infty [\widehat{m}_{11}U(s,p) + \widehat{m}_{12}\Phi(s,p) + \widehat{m}_{13}\Psi(s,p)]\sin(\xi s)\sin(\xi x)\mathrm{d}\xi\mathrm{d}s = \frac{\bar{\sigma}_0}{p}x, \quad x < a, \tag{34a}$$

$$\int_0^a \int_0^\infty [\widehat{m}_{21}U(s,p) + \widehat{m}_{22}\Phi(s,p) + \widehat{m}_{23}\Psi(s,p)]\sin(\xi s)\sin(\xi x)\mathrm{d}\xi\mathrm{d}s = \frac{\bar{D}_0}{p}x, \quad x < a, \tag{34b}$$

$$\int_0^a \int_0^\infty [\widehat{m}_{31}U(s,p) + \widehat{m}_{32}\Phi(s,p) + \widehat{m}_{33}\Psi(s,p)]\sin(\xi s)\sin(\xi x)\mathrm{d}\xi\mathrm{d}s = \frac{\bar{B}_0}{p}x, \quad x < a. \tag{34c}$$

Noting that

$$\lim_{\xi\to\infty} \widehat{m}_{kl}(\xi,p) = \bar{m}_{kl}, \quad k = 1, 2, 3, \quad l = 1, 2, 3, \tag{35}$$

and using the relation (Abramowitz and Stegun, 1965)

$$\int_0^\infty \sin(\xi s)\sin(\xi x)\mathrm{d}\xi = \frac{\pi}{2}\delta(s-x), \tag{36}$$

with $\delta(\bullet)$ being the Dirac delta function, Eq. (34) can be rewritten as

$$\bar{m}_{11}U(x,p) + \bar{m}_{12}\Phi(x,p) + \bar{m}_{13}\Psi(x,p) + \frac{2}{\pi}\int_0^a [R^A_{11}(s,x,p)U(s,p) + R^A_{12}(s,x,p)\Phi(s,p) + R^A_{13}(s,x,p)\Psi(s,p)]\mathrm{d}s = \frac{2\bar{\sigma}_0}{\pi p}x, \quad x < a, \tag{37a}$$

$$\bar{m}_{21}U(x,p) + \bar{m}_{22}\Phi(x,p) + \bar{m}_{23}\Psi(x,p) + \frac{2}{\pi}\int_0^a [R^A_{21}(s,x,p)U(s,p) + R^A_{22}(s,x,p)\Phi(s,p) + R^A_{23}(s,x,p)\Psi(s,p)]\mathrm{d}s = \frac{2\bar{D}_0}{\pi p}x, \quad x < a, \tag{37b}$$

$$\bar{m}_{31}U(x,p) + \bar{m}_{32}\Phi(x,p) + \bar{m}_{33}\Psi(x,p) + \frac{2}{\pi}\int_0^a [R^A_{31}(s,x,p)U(s,p) + R^A_{32}(s,x,p)\Phi(s,p) + R^A_{33}(s,x,p)\Psi(s,p)]\mathrm{d}s = \frac{2\bar{B}_0}{\pi p}x, \quad x < a, \tag{37c}$$

where

$$R^A_{kl}(s,x,p) = \int_0^\infty (\widehat{m}_{kl} - \bar{m}_{kl})\sin(\xi t)\sin(\xi x)\mathrm{d}\xi, \quad k = 1,2,3, \quad l = 1,2,3. \tag{38}$$

Hence, a system of coupled Fredholm integral equations for $U(x,p)$, $\Phi(x,p)$ and $\Psi(x,p)$ has been derived. Since the involved integrands in $R^A_{kl}(s,x,p)$ decay exponentially as $\xi \to \infty$, they are rapidly convergent and can easily be evaluated by truncating them as finite integrals.

3.1.2. Case B

We now consider Case B. From the boundary conditions in Eq. (8), we have

$$B_j(\xi,p) = -A_j(\xi,p)\coth(\gamma_j\xi h). \tag{39}$$

By an analogous treatment to the above, omitting the details, a system of coupled Fredholm integral equations for $U(x,p)$, $\Phi(x,p)$ and $\Psi(x,p)$ in this case take the following form:

Author's personal copy

$$\bar{m}_{11}U(x,p)+\bar{m}_{12}\Phi(x,p)+\bar{m}_{13}\Psi(x,p)+\frac{2}{\pi}\int_0^a[R^B_{11}(s,x,p)U(s,p)+R^B_{12}(s,x,p)\Phi(s,p)+R^B_{13}(s,x,p)\Psi(s,p)]\mathrm{d}s=\frac{2\bar{\sigma}_0}{\pi p}x,\quad x<a, \tag{40a}$$

$$\bar{m}_{21}U(x,p)+\bar{m}_{22}\Phi(x,p)+\bar{m}_{23}\Psi(x,p)+\frac{2}{\pi}\int_0^a[R^B_{21}(s,x,p)U(s,p)+R^B_{22}(s,x,p)\Phi(s,p)+R^B_{23}(s,x,p)\Psi(s,p)]\mathrm{d}s=\frac{2\bar{D}_0}{\pi p}x,\quad x<a, \tag{40b}$$

$$\bar{m}_{31}U(x,p)+\bar{m}_{32}\Phi(x,p)+\bar{m}_{33}\Psi(x,p)+\frac{2}{\pi}\int_0^a[R^B_{31}(s,x,p)U(s,p)+R^B_{32}(s,x,p)\Phi(s,p)+R^B_{33}(s,x,p)\Psi(s,p)]\mathrm{d}s=\frac{2\bar{B}_0}{\pi p}x,\quad x<a, \tag{40c}$$

where

$$R^B_{kl}(s,x,p)=\int_0^\infty(\breve{m}_{kl}-\bar{m}_{kl})\sin(\xi s)\sin(\xi x)\mathrm{d}\xi,\quad k=1,2,3,\quad l=1,2,3, \tag{41}$$

$$\breve{m}_{1l}(\xi,p)=\sum_{j=1}^4\beta_{1j}(p/\xi)\alpha_{lj}(p/\xi)\coth(\gamma_j\xi h),\quad l=1,2,3, \tag{42a}$$

$$\breve{m}_{kl}(\xi,p)=\sum_{j=1}^4\beta_{(k+1)j}(p/\xi)\alpha_{lj}(p/\xi)\coth(\gamma_j\xi h),\quad k=2,3,\quad l=1,2,3. \tag{42b}$$

3.2. Analysis on field intensity factors

Of interest to us is the magnetoelectroelastic behaviors induced by a penny-shaped crack, in particular in the vicinity of the crack fronts. Generally speaking, a closed-form solution of the resulting Fredholm integral equation for $U(x,p)$, $\Phi(x,p)$ and $\Psi(x,p)$ seems to be impossible due to the complexity of the involved kernels.

Because the integrands in Eq. (30) for Case A and in a similar equation (omitted here) for Case B are finite and continuous for any given values of ξ, the divergence of the integrals at the crack frontier must be due to the asymptotic behavior as $\xi\to\infty$. Carrying out the expansion for large ξ, and evaluating the integrals with respect to s by parts, we can, respectively, obtain the lower-order singular terms of the stress, electric displacement and magnetic induction on the crack plane. They are

$$\sigma^*_{zz}(r,p)=\int_0^\infty[\bar{m}_{11}U(a,p)+\bar{m}_{12}\Phi(a,p)+\bar{m}_{13}\Psi(a,p)]\cos(\xi a)J_0(\xi r)\mathrm{d}\xi+\mathrm{O}(1), \tag{43a}$$

$$D^*_z(r,p)=\int_0^\infty[\bar{m}_{21}U(a,p)+\bar{m}_{22}\Phi(a,p)+\bar{m}_{23}\Psi(a,p)]\cos(\xi a)J_0(\xi r)\mathrm{d}\xi+\mathrm{O}(1), \tag{43b}$$

$$B^*_z(r,p)=\int_0^\infty[\bar{m}_{31}U(a,p)+\bar{m}_{32}\Phi(a,p)+\bar{m}_{33}\Psi(a,p)]\cos(\xi a)J_0(\xi r)\mathrm{d}\xi+\mathrm{O}(1) \tag{43c}$$

for both Case A and Case B.

Defining the field intensity factors in the Laplace domain as follows

$$K^*_q(p)=\lim_{r\to a^+}\sqrt{2\pi(r-a)}q(r,p), \tag{44}$$

where $q(r,p)\equiv q(r,0,p)$ stands for σ^*_{zz}, D^*_z and B^*_z, respectively, and also noting that (Abramowitz and Stegun, 1965)

$$\int_0^\infty\cos(\xi a)J_0(\xi r)\mathrm{d}\xi=\frac{1}{\sqrt{r^2-a^2}},\quad r>a, \tag{45}$$

Author's personal copy

we then find that the intensity factors of stress, electric displacement and magnetic induction in the Laplace domain can be expressed as

$$K_\sigma^*(p) = \frac{\bar{m}_{11}U(a,p) + \bar{m}_{12}\Phi(a,p) + \bar{m}_{13}\Psi(a,p)}{a}\sqrt{\pi a}, \tag{46a}$$

$$K_D^*(p) = \frac{\bar{m}_{21}U(a,p) + \bar{m}_{22}\Phi(a,p) + \bar{m}_{23}\Psi(a,p)}{a}\sqrt{\pi a}, \tag{46b}$$

$$K_B^*(p) = \frac{\bar{m}_{31}U(a,p) + \bar{m}_{32}\Phi(a,p) + \bar{m}_{33}\Psi(a,p)}{a}\sqrt{\pi a}. \tag{46c}$$

Similarly, in the Laplace domain, the field intensity factors associated with the crack opening displacement $u_z^*(r,p)$, electric potential $\phi^*(r,p)$ and magnetic potential $\psi^*(r,p)$ across the crack near the crack front are defined and easily derived from Eq. (26) as

$$K_{\mathrm{COD}}^*(p) \triangleq \lim_{r\to a^-}\sqrt{\frac{\pi}{2(a-r)}}u_z^*(r,p) = \sqrt{\pi a}\frac{U(a,p)}{a}, \tag{47a}$$

$$K_\phi^*(p) \triangleq \lim_{r\to a^-}\sqrt{\frac{\pi}{2(a-r)}}\phi^*(r,p) = \sqrt{\pi a}\frac{\Phi(a,p)}{a}, \tag{47b}$$

$$K_\psi^*(p) \triangleq \lim_{r\to a^-}\sqrt{\frac{\pi}{2(a-r)}}\psi^*(r,p) = \sqrt{\pi a}\frac{\Psi(a,p)}{a}. \tag{47c}$$

The intensity factors in the time domain can then be obtained by

$$K_q(t) = \frac{1}{2\pi i}\int_{\mathrm{Br}} K_q^*(p)e^{pt}dp, \quad q = \sigma, D, B, COD, \phi, \psi, \tag{48}$$

where Br denotes Bromwich path of integration.

Eqs. (46) and (47) together with Eq. (37) or (40) indicate that all the field intensity factors depend directly on the material constants, the thickness of the layer, and the mangnetoelectromechanical impact loadings applied on the crack surfaces.

It should be noted that the above results can easily be reduced to those corresponding to the static case, which in fact have not been reported before. In this case, the stress, electric displacement and magnetic induction on the crack plane become

$$\sigma_{zz}(r) = -\int_0^a\int_0^\infty [m_{11}U(s) + m_{12}\Phi(s) + m_{13}\Psi(s)]\xi\sin(\xi s)J_0(\xi r)\mathrm{d}\xi\mathrm{d}s, \tag{49a}$$

$$D_z(r) = -\int_0^a\int_0^\infty [m_{21}U(s) + m_{22}\Phi(s) + m_{23}\Psi(s)]\xi\sin(\xi s)J_0(\xi r)\mathrm{d}\xi\mathrm{d}s, \tag{49b}$$

$$B_z(r) = -\int_0^a\int_0^\infty [m_{31}U(s) + m_{32}\Phi(s) + m_{33}\Psi(s)]\xi\sin(\xi s)J_0(\xi r)\mathrm{d}\xi\mathrm{d}s, \tag{49c}$$

where

$$m_{1l} = \sum_{j=1}^4 \beta_{1j}(0)\alpha_{lj}(0)\tanh(\gamma_j\xi h), \quad l = 1, 2, 3, \tag{50a}$$

$$m_{kl}(\xi) = \sum_{j=1}^4 \beta_{(k+1)j}(0)\alpha_{lj}(0)\tanh(\gamma_j\xi h), \quad k = 2, 3, \quad l = 1, 2, 3 \tag{50b}$$

for Case A, and

$$m_{1l} = \sum_{j=1}^4 \beta_{1j}(0)\alpha_{lj}(0)\coth(\gamma_j\xi h), \quad l = 1, 2, 3, \tag{51a}$$

Author's personal copy

$$m_{kl}(\xi)=\sum_{j=1}^{4}\beta_{(k+1)j}(0)\alpha_{lj}(0)\coth(\gamma_j\xi h),\quad k=2,3,\quad l=1,2,3 \tag{51b}$$

for Case B. Thus, the field intensity factors can finally be given as

$$K_\sigma=\frac{\bar{m}_{11}U(a)+\bar{m}_{12}\Phi(a)+\bar{m}_{13}\Psi(a)}{a}\sqrt{\pi a}, \tag{52a}$$

$$K_D=\frac{\bar{m}_{21}U(a)+\bar{m}_{22}\Phi(a)+\bar{m}_{23}\Psi(a)}{a}\sqrt{\pi a}, \tag{52b}$$

$$K_B=\frac{\bar{m}_{31}U(a)+\bar{m}_{32}\Phi(a)+\bar{m}_{33}\Psi(a)}{a}\sqrt{\pi a}, \tag{52c}$$

and

$$K_{\mathrm{COD}}=\frac{U(a)}{a}\sqrt{\pi a},\quad K_\phi=\frac{\Phi(a)}{a}\sqrt{\pi a},\quad K_\psi=\frac{\Psi(a)}{a}\sqrt{\pi a}, \tag{53}$$

where $U(x)$, $\Phi(x)$ and $\Psi(x)$ satisfy the following equations:

$$\bar{m}_{11}U(x)+\bar{m}_{12}\Phi(x)+\bar{m}_{13}\Psi(x)+\frac{2}{\pi}\int_0^a[R_{11}(s,x)U(s)+R_{12}(s,x)\Phi(s)+R_{13}(s,x)\Psi(s)]\mathrm{d}s=\frac{2\bar{\sigma}_0}{\pi}x,\quad x<a, \tag{54a}$$

$$\bar{m}_{21}U(x)+\bar{m}_{22}\Phi(x)+\bar{m}_{23}\Psi(x)+\frac{2}{\pi}\int_0^a[R_{21}(s,x)U(s)+R_{22}(s,x)\Phi(s)+R_{23}(s,x)\Psi(s)]\mathrm{d}s=\frac{2\bar{D}_0}{\pi}x,\quad x<a, \tag{54b}$$

$$\bar{m}_{31}U(x)+\bar{m}_{32}\Phi(x)+\bar{m}_{33}\Psi(x)+\frac{2}{\pi}\int_0^a[R_{31}(s,x)U(s)+R_{32}(s,x)\Phi(s)+R_{33}(s,x)\Psi(s)]\mathrm{d}s=\frac{2\bar{B}_0}{\pi}x,\quad x<a, \tag{54c}$$

with $R_{ij}(s,x)$ referring to $R_{ij}^{A}(s,x,0)$ for Case A and to $R_{ij}^{B}(s,x,0)$ for Case B.

Eqs. (52) and (53) together with Eqs. (54) imply that, similar to the dynamic impact problem, all the field intensity factors under static loadings are also related to the material constants, thickness of the layer and the magnetoelectromechanical loadings applied on the crack surfaces.

From Eq. (54), it is further observed that for the limiting case of an infinite magnetoelectroelastic space, $R_{kl}(s,x)\to 0$ follows $h\to\infty$. Thus, the governing Fredholm integral equations can be transformed into a system of linear algebraic equations, from which the unknown functions $U(x)$, $\Phi(x)$ and $\Psi(x)$ can be solved directly. Further substituting the obtained $U(a)$, $\Phi(a)$ and $\Psi(a)$ into Eqs. (52) and (53) yields

$$K_\sigma=\frac{2}{\pi}\sqrt{\pi a}\bar{\sigma}_0,\quad K_D=\frac{2}{\pi}\sqrt{\pi a}\bar{D}_0,\quad K_B=\frac{2}{\pi}\sqrt{\pi a}\bar{B}_0. \tag{55}$$

The results given by Eq. (55) are very simple and interesting, which shows that for an infinite magnetoelectroelastic medium with a magnetoelectrically impermeable penny-shaped crack, the stress, electric displacement and magnetic induction intensity factors depend respectively on the mechanical loading, electric displace and magnetic induction applied on the crack surfaces. This is quite different to the case of finite layer even in the static case.

4. Magnetoelectrically permeable cracks

It is noted that for the magnetoelectrically permeable crack case, both electric and magnetic potentials are continuous across the crack surfaces. Thus, by a similar method to the magnetoelectrically impermeable case, the problem can be reduced to the following Fredhom integral equation

Author's personal copy

$$\bar{m}_{11}U(x,p)+\frac{2}{\pi}\int_0^a R_{11}(s,x,p)U(s,p)\mathrm{d}s=\frac{2\bar{\sigma}_0}{\pi p}x,\quad x<a, \tag{56}$$

with $R_{11}(s,x,p)$ referring to $R_{11}^A(s,x,p)$ for Case A and to $R_{11}^B(s,x,p)$ for Case B. The electric displacement and magnetic induction on the crack surfaces in the Laplace domain can be derived as

$$D_z^*(r,p)=-\int_0^a\int_0^\infty \hat{m}_{21}U(s,p)\xi\sin(\xi s)J_0(\xi r)\mathrm{d}\xi\mathrm{d}s+\frac{\bar{D}_0}{p}, \tag{57a}$$

$$B_z^*(r,p)=-\int_0^a\int_0^\infty \hat{m}_{31}U(s,p)\xi\sin(\xi s)J_0(\xi r)\mathrm{d}\xi\mathrm{d}s+\frac{\bar{B}_0}{p}, \tag{57b}$$

where

$$\hat{m}_{21}=\begin{cases}\overset{\frown}{m}_{21}, & \text{Case A},\\ \overset{\smile}{m}_{21}, & \text{Case B}.\end{cases} \tag{58}$$

The field intensity factors in the time domain can finally be expressed as

$$K_{\mathrm{COD}}(t)=\frac{U(a,t)}{a}\sqrt{\pi a},\quad K_\phi(t)=0,\quad K_\psi(t)=0, \tag{59a}$$

$$K_\sigma(t)=\bar{m}_{11}K_{\mathrm{COD}}(t),\quad K_D(t)=\bar{m}_{21}K_{\mathrm{COD}}(t),\quad K_B(t)=\bar{m}_{31}K_{\mathrm{COD}}(t). \tag{59b}$$

Eq. (59) indicates that the four field intensity factors of COD, stress, electric displacement and magnetic induction are dependent on each other through material constants and thickness of the layer. This phenomenon has been partially observed for the 2D static problem in an infinite magnetoelectroelastic medium (Gao et al., 2003). In addition, both $\bar{D}_0$ and $\bar{B}_0$ have no effects on these field intensity factors. Moreover, as shown in (59a), both electric and magnetic potential intensity factors vanish.

Similarly, further analysis on static or infinite cases can easily be carried out as well. For example, for an infinite magnetoelectroelastic medium under static loadings, the field intensity factors can be reduced to

$$K_{\mathrm{COD}}=\frac{2}{\pi\bar{m}_{11}}\sqrt{\pi a}\bar{\sigma}_0,\quad K_\phi=0,\quad K_\psi=0, \tag{60a}$$

$$K_\sigma=\bar{m}_{11}K_{\mathrm{COD}},\quad K_D=\bar{m}_{21}K_{\mathrm{COD}},\quad K_B=\bar{m}_{31}K_{\mathrm{COD}}, \tag{60b}$$

which indicates that for a magnetoelectrically permeable crack embedded in an infinite magnetoelectroelastic body, unlike the stress intensity factor, the COD intensity factor depends directly on both the material property and the corresponding mechanical loading applied on the crack surfaces. This, in some extent, implies the COD intensity factor could be more reasonable than stress intensity factor as a fracture parameter.

5. Numerical results

According to the classical COD fracture criterion for a three-dimensional elastic body, crack starts to grow when the COD intensity factor exceeds the critical value under the applied loading. For a magnetoelectroelastic material, not only mechanical loading but also magnetic and electrical loadings can cause a crack to open and even to propagate. In this section, some numerical results are given to examine the effects of the crack surface conditions, layer thickness and applied magnetic and/or electric fields on the COD intensity factors near the crack front.

Numerical calculations are carried out for a penny-shaped crack in a $BaTiO_3$–$CoFe_2O_4$ composite. The density of the composite is taken as $\rho=5.5\times10^3\ \mathrm{kg/m^3}$ and the other material properties are taken from Wang and Mai (2007).

Without loss of generality, in all our numerical examples, it is assumed that $\sigma_0=4.2\times10^6\ \mathrm{N/m^2}$ for Case A and $\sigma_h=4.2\times10^6\ \mathrm{N/m^2}$ for Case B, where $\sigma_h=c_{33}\,u_h/h$ represents the average stress in the absence of both applied magnetic and electric fields in Case B. Numerical results are plotted in Figs. 2–7, where K_0 represents the static COD intensity factor for an infinite magnetoelectroelastic solid under mechanical loading only (i.e., $\sigma_0H(t)$ or σ_0 for Case A, $\sigma_hH(t)$ or σ_h for Case B, respectively) in the case of magnetoelectrically impermeable

Author's personal copy

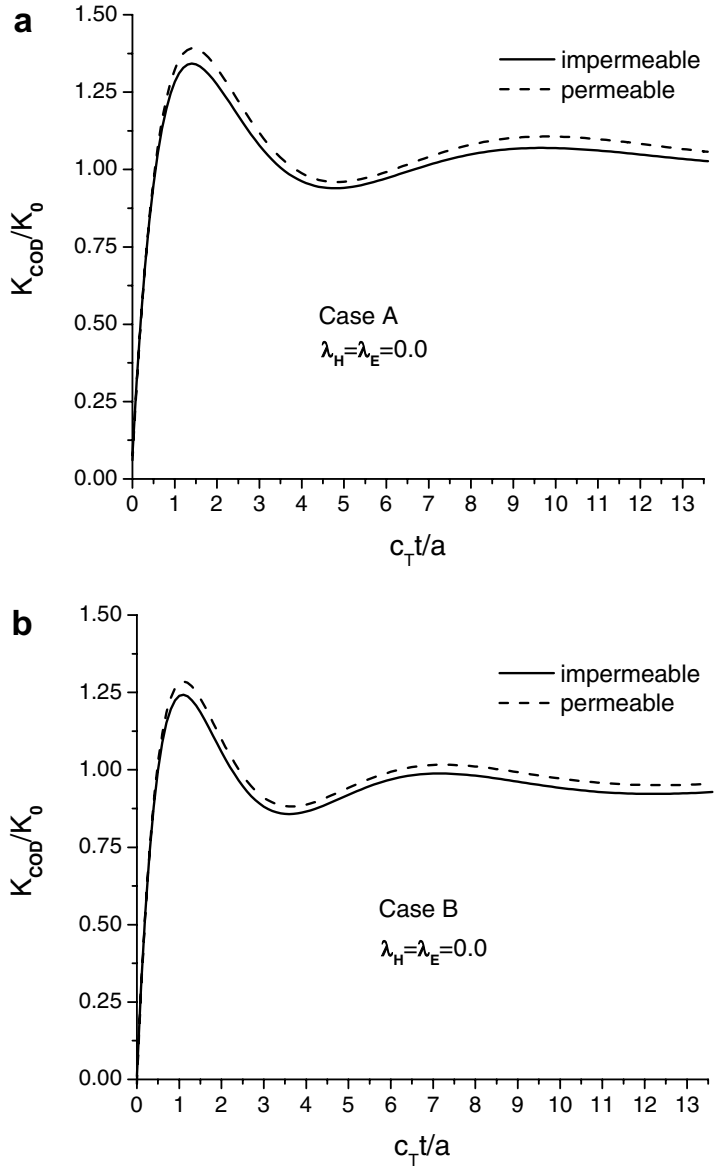

Fig. 2. Variation of normalized dynamic COD intensity factors with normalized time for magnetoelectrically impermeable and permeable cracks as $h/a = 2.0$: (a) Case A, (b) Case B.

crack surface. For Case A, the loading combination parameters λ_H and λ_E are determined as $\lambda_H = f_{33}H_0/\sigma_0$ and $\lambda_E = e_{33}E_0/\sigma_0$, which are used to reflect the corresponding loading combinations between magnetic and mechanical loadings, and between electrical and mechanical loadings, respectively. Similarly, in Case B, the loading combination parameters $\lambda_H = f_{33}\psi_h/(c_{33}u_h)$ and $\lambda_E = e_{33}\phi_h/(c_{33}u_h)$ are respectively introduced to reflect the loading combinations between magnetic and mechanical loadings, and between electrical and mechanical loadings. For the impact problem, the time is normalized by $c_T t/a$, where c_T is the shear wave velocity in magnetoelectroelastic body, i.e.,

$$c_T = \sqrt{[c_{44} + (\varepsilon_{11}f_{15}^2 - 2e_{15}f_{15}g_{11} + \mu_{11}e_{15}^2)/(\mu_{11}\varepsilon_{11} - g_{11}^2)]/\rho}. \tag{61}$$

The Laplace inversion is carried out by the numerical method proposed by Miller and Guy (1966), with the detail being listed in Appendix A for the sake of easy reference. It should be pointed out that the parameters β, δ and N are selected such that the physical quantities in the time domain can be best described within a

Author's personal copy

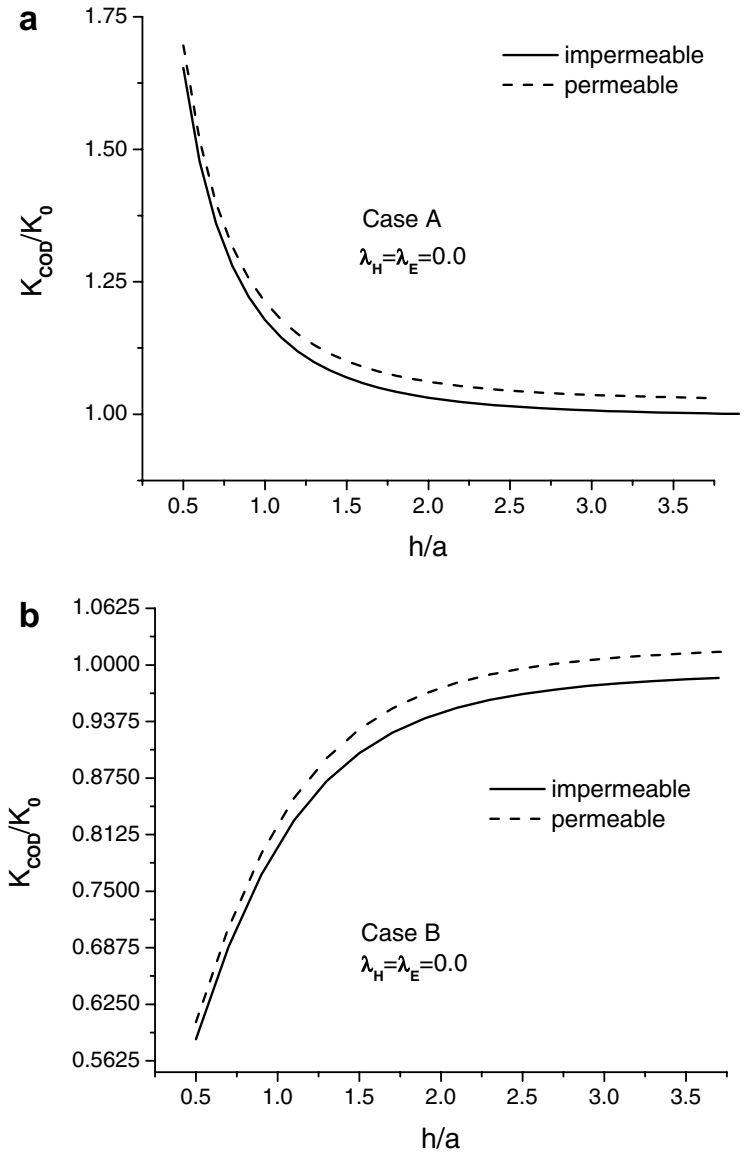

Fig. 3. Variation of normalized COD intensity factors with normalized layer thickness for static problems of magnetoelectrically impermeable and permeable cracks: (a) Case A, (b) Case B.

particular period of time, and in the present study, the optimal parameters β, δ and N are selected to be 0, 250 and 9, respectively.

Fig. 2 compares the normalized dynamic K_{COD} between magnetoelectrically impermeable and permeable cracks for $h/a = 2.0$ in the absence of magnetoelectrical loadings (i.e., $\lambda_H = \lambda_E = 0$). The peak values corresponding to the magnetoelectrically impermeable crack are smaller than those corresponding to the permeable crack for both Cases A and B (This phenomenon is further demonstrated in Fig. 3). There is no other distinct difference between the two kinds of crack surface conditions. As pointed out before, for the magnetoelectrically permeable crack, both magnetic and electrical loadings have no contributions to K_{COD} for Case A. However, it is easily seen that, different from Case A, for Case B, both the magnetic and electric fields have great effects on the normalized K_{COD}, and in fact, the COD intensity factor under the applied magnetic and electrical loadings can be expressed as $K_{\mathrm{COD}}^{\mathrm{Per,caseB},\lambda} = (1 - \lambda_H - \lambda_E)K_{\mathrm{COD}}^{\mathrm{Per,caseB},\lambda,0}$, where $K_{\mathrm{COD}}^{\mathrm{Per,caseB},\lambda,0}$ is the corresponding COD intensity factor under mechanical displacement impact only.

Fig. 3 shows the effect of the layer thickness on the static K_{COD}. It is interesting that the COD intensity factors for Case A and Case B tend to the ones in the corresponding infinite magnetoelectroelastic body with

Author's personal copy

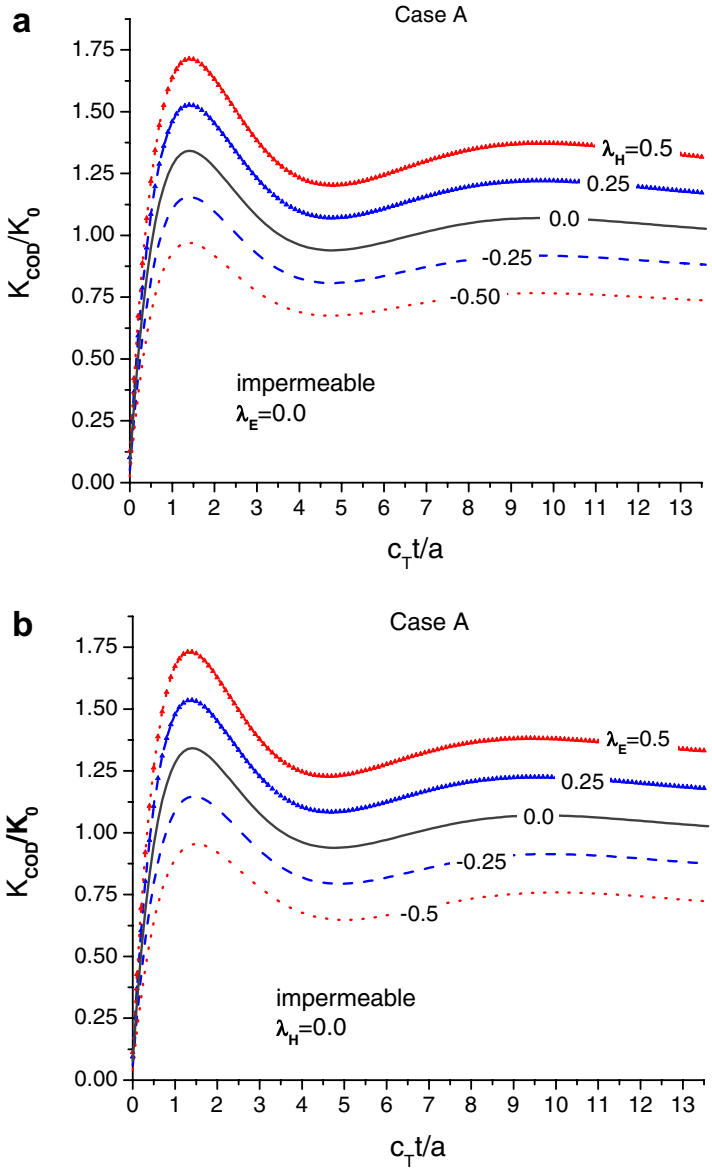

Fig. 4. Variation of normalized dynamic COD intensity factors with normalized time for magnetoelectrically impermeable cracks in Case A as $h/a = 2.0$ under magnetic impacts in (a) and under electrical impacts in (b).

increasing h/a; on the other hand, the K_{COD} decreases monotonically for Case A and increases monotonically for Case B . In addition, the K_{COD} is faster to approach the corresponding value in the unbounded medium for Case A than for Case B. From Fig. 3, it is also observed that for the impermeable cracks, the normalized K_{COD} in fact tends to one, which in a certain sense implies our results are correct.

Figs. 4 and 5 show the effects of the magnetic and electrical impacts on the normalized dynamic K_{COD} for the magnetoelectrically impermeable crack. As shown in Fig. 4(a) and (b), within the ranges of our calculation, both negative magnetic and electrical loadings inhibit crack propagation and growth for Case A, whilst both positive magnetic and electrical loadings enhance crack propagation. The effect of the electrical loading on K_{COD} for the magnetoelectroelastic body is in agreement with the corresponding experimental result for piezoelectric ceramic (Park and Sun, 1995). However, it is found, from Fig. 5(a) and (b), that the trends are reversed for the prescribed displacement case, i.e., both the applied positive magnetic and electric fields can hinder crack growth, and either negative magnetic or electric field promotes crack growth. This trend was also identified in previous research (Wang and Singh, 1997; Shindo et al., 2002; Li and Lee, 2004). Figs. 4 and 5 further indicate that both the magnetic and electrical loadings nearly have no effects on the time to reach the

Author's personal copy

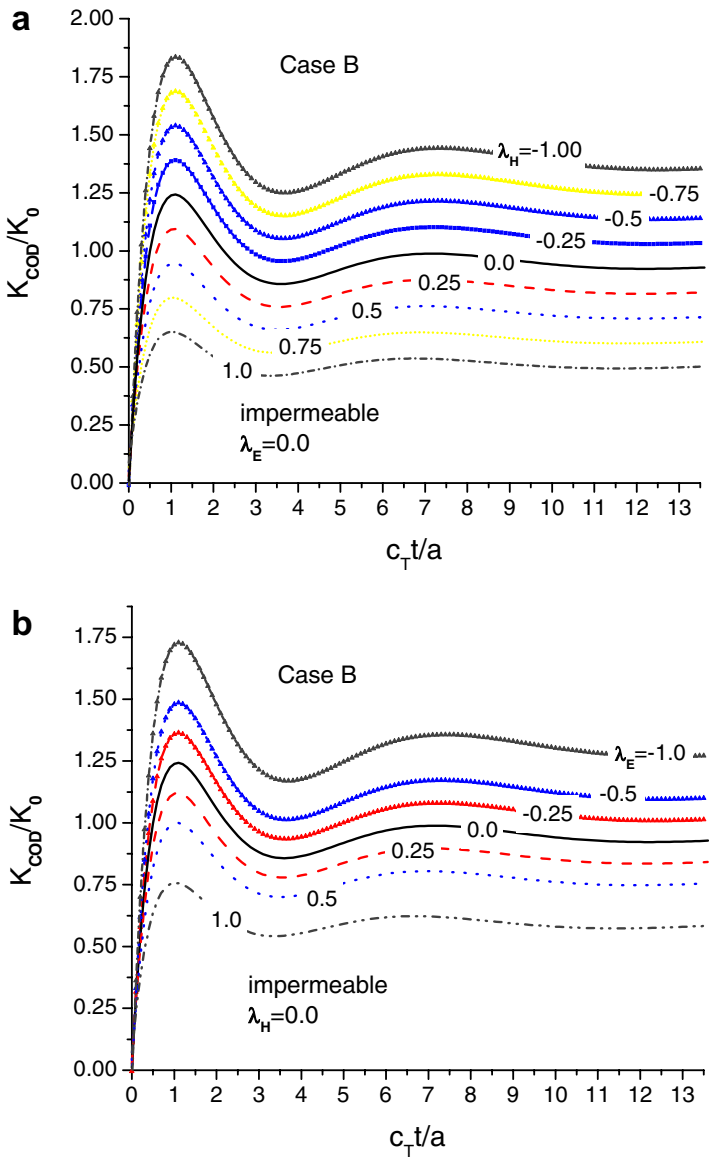

Fig. 5. Variation of normalized dynamic COD intensity factors with normalized time for magnetoelectrically impermeable cracks in Case B as $h/a = 2.0$ under magnetic impacts in (a) and under electrical impacts in (b).

corresponding peak values of K_{COD}. However, by comparing Fig. 4 with Fig. 5, one can further note that the peak value of K_{COD} generally appears at $c_T t/a \approx 1.50$ for Case A and at $c_T t/a \approx 1.0$ for Case B, which implies that the time to reach the peak values is different for the two kinds of boundary conditions (Cases A and B).

Figs. 6 and 7 further show the effect of both magnetic and electrical loadings on the static K_{COD} for Case A and Case B, respectively. Comparing Figs. 4 with 6, and/or Figs. 5 with 7, it is found that, as expected, the dynamic K_{COD} indeed tends the corresponding static one. In addition, Fig. 6 also shows that for Case A, for a fixed value of h/a, there is a negative critical value under both magnetic and electrical loadings. For a given λ_E (or λ_H), when λ_H (or λ_E) is less than the corresponding critical value, the calculated K_{COD} is less than zero. It perhaps should be explained that the crack is actually closed at this moment. Similarly, as shown in Fig. 7, there are corresponding critical loadings for Case B as well. However, for Case B, the critical loadings corresponding to both magnetic and electrical loadings are positive. In addition, Figs. 6(a) and 7(a) also indicate that for the material considered here, the layer thickness has neglected effect on the magnetic critical loadings for both Case A and Case B, and the absolute-valued magnetic critical loadings are almost identical, i.e., $\lambda_{H(cr)} \approx -2.0$ for Case A and $\lambda_{H(cr)} \approx 2.0$ for Case B. However, different from the magnetic critical loading

Author's personal copy

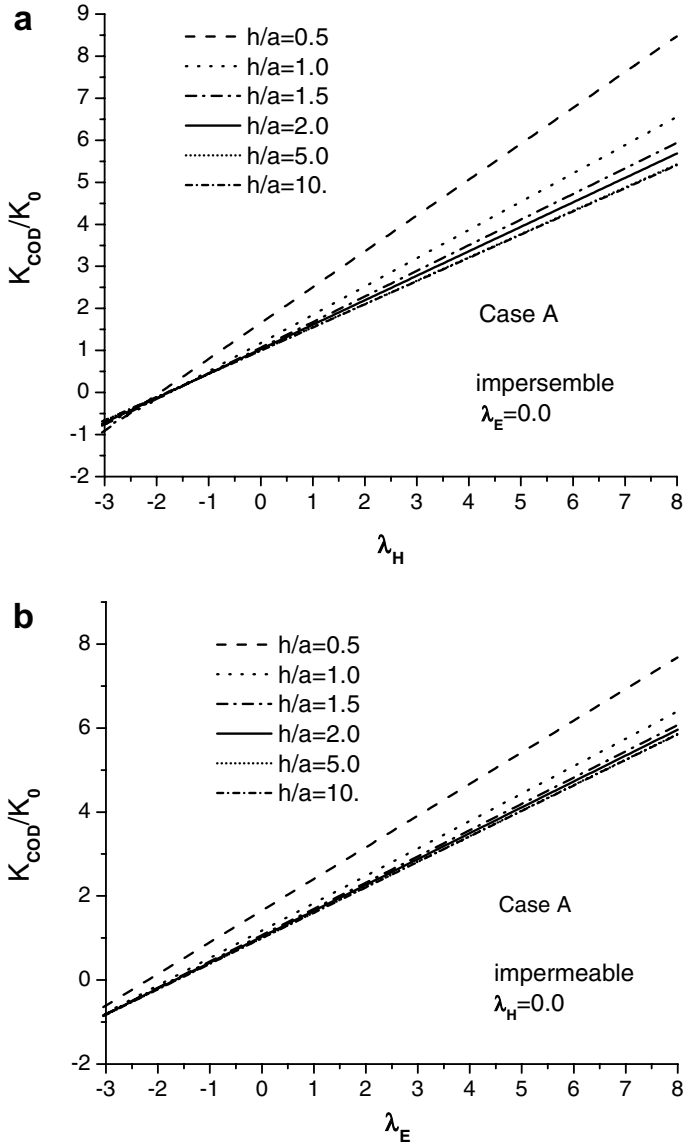

Fig. 6. Normalized COD intensity factors for static problems of magnetoelectrically impermeable cracks under different (a) magnetic and (b) electrical loadings in Case A.

case, as shown in Figs. 6(b) and 7(b), the layer thickness has significant influence on the electrical critical loading. In general, observation of Figs. 4–7 suggests that except for the crack surface condition, magnetoelectroelastic boundary conditions also play a significant role on the crack propagation in magnetoelectroelastic materials.

We finally point out that our formulations have been verified to be correct, and in particular, for the reduced simple case, our solutions are the same as previously known results. For example, for the static COD intensity factors of an electrically impermeable penny-shaped crack situated in piezoelectric ceramic layer (PZT-5H) for Case A, i.e., at the layer surfaces, we have

$$\sigma_{zz}(r,h)=\sigma_0, u_r(r,h)=0, \quad E_z(r,h)=E_0, \quad r<\infty. \tag{62}$$

The material properties of PZT-5H are listed in Li and Lee (2004). For the sake of comparison, the COD intensity factors are normalized by K_* corresponding the value of K_{COD} under $E_0=0$. The normalized COD intensity factor curvers are given in Fig. 8, which are the same as those in Fig. 3 of Li and Lee (2004). This is one of the numerical examples that we used to verify our formulations.

Author's personal copy

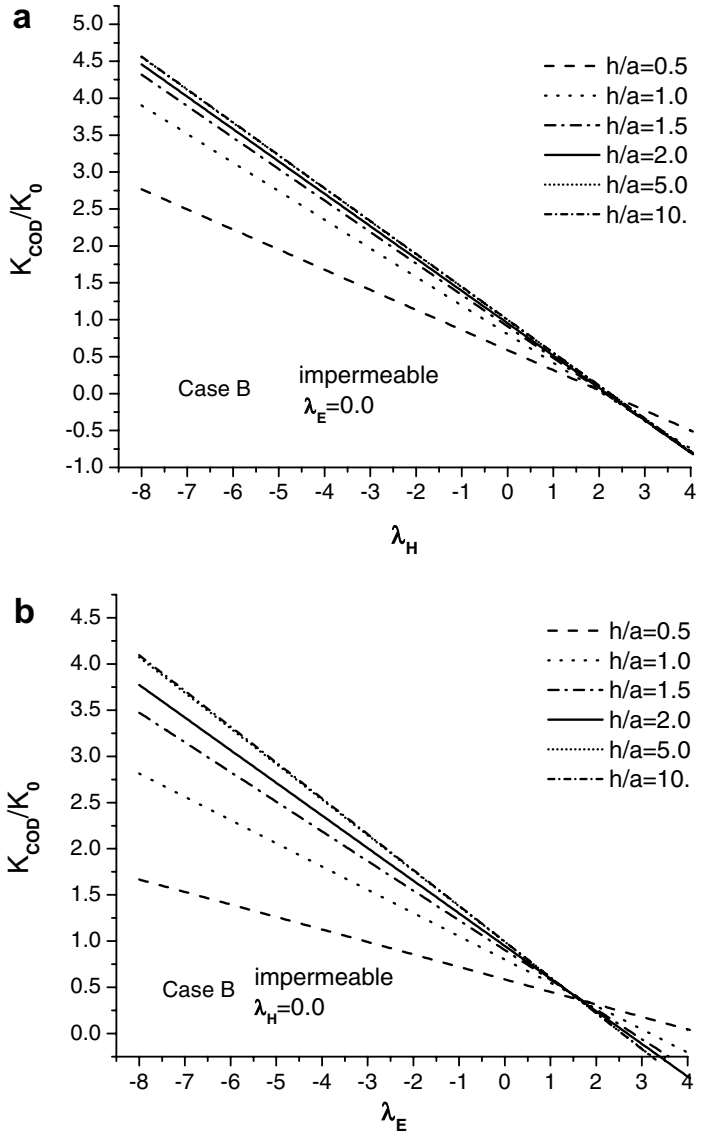

Fig. 7. Normalized COD intensity factors for static problems of magnetoelectrically impermeable cracks under different (a) magnetic and (b) electrical loadings in Case B.

6. Conclusions

In this paper, a penny-shaped crack in a magnetoelectroelastic layer is investigated. Two kinds of impact loadings, i.e., the prescribed extended stress and displacement impacts, are considered. Two kinds of crack surface conditions, i.e., the magnetoelectrically impermeable and permeable cracks, are adopted. From our analysis and the corresponding numerical results, the following conclusions can be drawn:

(1) The dynamic COD intensity factors exist peak values for both Case A and Case B, and both the magnetic and electrical impact loadings have no obvious effects on the time to reach the corresponding peak values. However, for Case A, the normalized time of reaching the peak value is slightly larger than the one for Case B.
(2) For the material considered here, under only mechanical loadings (i.e., σ_0 for Case A and σ_h for Case B), the COD intensity factors of the magnetoelectrically permeable crack are generally larger than those corresponding to the impermeable crack for both Case A and Case B.

Author's personal copy

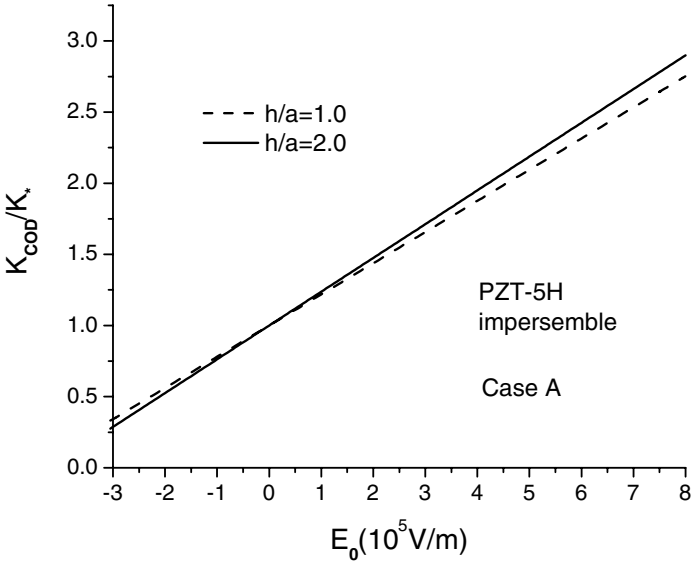

Fig. 8. Normalized COD intensity factors for static problems of electrically impermeable penny-shaped crack under different electrical loadings in Case A.

(3) For the magnetoelectrically impermeable crack, according to the maximum COD criterion, for Case A, both positive magnetic and electrical loadings always enhance the crack propagation, and both negative magnetic and electric fields impede crack propagation. For Case B, both magnetic and electrical loadings have quite reversed effects on the crack propagation and growth.
(4) For the magnetoelectrically permeable crack, both magnetic and electric fields have no apparent effects on the COD intensity factors for Case A. However, for Case B, except for mechanical loading (σ_h), the COD depends strongly on both the magnetic and electrical loadings. We also notice that in order to keep the crack open, the combination loadings applied on the layer should satisfy the condition $\lambda_H + \lambda_E < 1.0$.
(5) For the given mechanical loadings, with increasing layer thickness, the COD intensity factors monotonically decrease for Case A and monotonically increase for Case B. Finally, they all approach the limiting values corresponding to the infinite magnetoelectroelastic body.

Acknowledgement

The work was supported by the National Natural Science Fund of China and Natural Science Fund of Hebei Province, and partially by AFOSR/AFRL, ARO/ARL, USA.

Appendix A

According to Miller and Guy (1966), if the Laplace transform of the time-domain function $f(t)$ is $f^*(p)$, then the Laplace variable p can be evaluated at the following points

$$p = \delta(\beta + 1 + n), \quad n = 1, 2, \cdots. \tag{A.1}$$

If we further determine the coefficients C_m from the following set of equations:

$$\delta f^*(\delta(\beta + 1 + n)) = \sum_{m=0}^{n} \frac{C_m n!}{(\beta + n + 1)(\beta + n + 2)\cdots(\beta + n + 1 + m)(n - m)!}, \tag{A.2}$$

where $\delta > 0$ and $\beta > -1.0$. Then, the time-domain function$f(t)$can be approximately expressed by

Author's personal copy

$$f(t) = \sum_{m=0}^{N-1} C_m P_m^{(0,\beta)}(2e^{-\delta t} - 1), \tag{A.3}$$

where $P_m^{(0,\beta)}(x)$ is a Jacobi polynomial and N is the number of terms employed.

References

Abramowitz, M., Stegun, I.A., 1965. Handbook of Mathematical Functions: with Formulas, Graphs, and Mathematical Tables. Dover Publications, New York.

Avellaneda, M., Harshe, G., 1994. Magnetoelectric effect in piezoelectric/ magnetostrictive multiplayer (2–2) composites. J. Intell. Mater. Syst. Struct. 5, 501–513.

Benveniste, Y., 1995. Magnetoelectric effect in fibrous composites with piezoelectric and piexomagnetic phases. Phys. Rev. B 51, 16424–16427.

Chue, C.H., Liu, T.J.C., 2005. Magneto-electro-elastic antiplane analysis of a biomaterial $BaTiO_3$–$CoFe_2O_4$ composite wedge with an interface crack. Theo. Appl. Frac. Mech. 44, 275–296.

Du, J.K., Shen, Y.P., Ye, D.Y., Yue, F.R., 2004. Scattering of anti-plane shear waves by a partially debonded magneto-electro-elastic circular cylindrical inhomogeneity. Int. J. Eng. Sci. 42, 887–913.

Feng, W.J., Su, R.K.L., 2006. Dynamic internal crack problem of a functionally graded magneto-electro-elastic strip. Int. J. Solids Struct. 43, 5196–5216.

Gao, C.F., Tong, P., Zhang, T.Y., 2003. Interfacial crack problems in magneto-electroelastic solids. Int. J. Engn. Sci. 41, 2105–2121.

Harshe, G., Dougherty, J.P., Newnham, R.E., 1993. Theoretical modeling of 3–0/0–3 magnetoelectric composites. Int. J. Appl. Electromagn. Mech. 4, 161–171.

Hu, K.Q., Li, G.Q., Zhong, Z., 2006. Fracture of a rectangular piezoelectromagnetic body. Mech. Res. Commun. 33, 482–492.

Huang, J.H., Kuo, W.S., 1997. The analysis of piezoelectric/piezomagnetic composite materials containing an ellipsoidal inhomogeneity. J. Appl. Phys. 81, 1378–1386.

Kirchner, H.O.K., Alshits, I., 1996. Elastically anisotropic angularly inhomogeneous media II. The Green's function for piezoelectric, piezomagnetic and magnetoelectric media. Philos. Mag. A 74, 861–885.

Li, J.Y., Dunn, M.L., 1998. Micromechanics of magneto-electro-elastic composite materials: average fields and effective behavior. J. Intell. Mater. Syst. Struct. 9, 404–416.

Li, R., Kardomateas, G.A., 2006. The Mode III interface crack in piezo-electro-magneto-elastic dissimilar bimaterials. ASME J. Appl. Mech. 73, 220–227.

Li, X.F., Lee, K.Y., 2004. effects of electric field on crack growth for a penny-shaped dielectric crack in a piezoelectric layer. J. Mech. Phys. Solids 52, 2079–2100.

Miller, M.K., Guy, W.T., 1966. Numerical inversion of Laplace transform by use of Jacobi polynomial. SIAM J. Numer. Anal. 3, 624–635.

Nan, C.W., 1994. Magneto-electric effect in composites of piezoelectric and piezomagnetic phases. Phys. Rev. B 50, 6082–6088.

Niraula, O.P., Wang, B.L., 2006. A magneto-electro-elastic material with a penny-shaped crack subjected to temperature loading. Acta Mech. 187, 151–168.

Park, S., Sun, C.T., 1995. Fracture criteria for piezoelectric ceramics. J. Am. Ceram. Soc. 78, 1475–1480.

Shindo, Y., Murakami, H., Horiguchi, K., Narita, F., 2002. Evaluation of electric fracture properties of piezoelectric ceramics using the finite elecment and single-edge precraked-beam methods. J. Am. Ceram. Soc. 85, 1243–1248.

Sih, G.C., Yu, H.Y., 2005. Volume fraction effect of magnetoelectroelastic composite on enhancement and impediment of crack growth. Comp. Struct. 68, 1–11.

Soh, A.K., Liu, J.X., 2005. On the constitutive equations of magnetoelectroelastic solids. J. Intell. Mater. Syst. Struct. 16, 202–597.

Song, Z.F., Sih, G.C., 2003. Crack initiation behavior in magnetoelectroelastic composite under in-plane deformation. Theor. Appl. Frac. Mech. 39, 189–207.

Su, R.K.L., Feng, W.J., Liu, J., 2007. Transient response of interface cracks between dissimilar magneto-electro-elastic strips under out-of-plane mechanical and in-plane magneto-electrical impact loads. Comp. Struct. 78, 119–128.

Tian, W.Y., Gabbert, U., 2004. Multiple crack interaction problem in magnetoelectroelastic solids. Eur. J. Mech. A/Solids 23, 599–614.

Tian, W.Y., Gabbert, U., 2005. Macro-crack–micro-crack problem interaction problem in magnetoelectroelastic solids. Mech. Mater. 37, 565–592.

Tian, W.Y., Rajapakse, R.K.N.D., 2005. Fracture analysis of magnetoelectroelastic solids by using path independent integrals. Int. J. Frac. 131, 311–335.

Wang, B.L., Han, J.C., Mai, Y.W., 2006. Mode III fracture of a magnetoelectroelastic layer: exact solution and discussion of the crack face electromagnetic boundary conditions. Int. J. Frac. 139, 27–38.

Wang, B.L., Mai, Y.W., 2007. Applicability of the crack-face electromagnetic boundary conditions for fracture of magnetoelectroelastic materials. Int. J. Solids Struct. 44, 387–398.

Wang, H., Singh, R.N., 1997. Crack propagation in piezoelectric ceramics: effects of applied electric fields. J. Appl. Phys. 81, 7471–7479.

Zhao, M.H., Yang, F., Liu, T., 2006. Analysis of a penny-shaped crack in a magneto-electro-elastic medium. Philos. Mag. 86, 4397–4416.

Zhou, Z.G., Wang, B., Sun, Y.G., 2004. Two collinear interface cracks in magneto-electro-elastic composites. Int. J. Eng. Sci. 42, 1155–1167.